Piezoelectric trace vapor calibrator

R. Michael Verkouteren and Greg Gillen
Surface and Microanalysis Science Division, National Institute of Standards and Technology, Gaithersburg, Maryland 20899

David W. Taylor
MicroFab Technologies, Inc., 1104 Summit Avenue, Suite 110, Plano, Texas 75074

(Received 19 April 2006; accepted 29 June 2006; published online 14 August 2006)

The design and performance of a vapor generator for calibration and testing of trace chemical sensors are described. The device utilizes piezoelectric ink-jet nozzles to dispense and vaporize precisely known amounts of analyte solutions as monodisperse droplets onto a hot ceramic surface, where the generated vapors are mixed with air before exiting the device. Injected droplets are monitored by microscope with strobed illumination, and the reproducibility of droplet volumes is optimized by adjustment of piezoelectric wave form parameters. Complete vaporization of the droplets occurs only across a 10 °C window within the transition boiling regime of the solvent, and the minimum and maximum rates of trace analyte that may be injected and evaporated are determined by thermodynamic principles and empirical observations of droplet formation and stability. By varying solution concentrations, droplet injection rates, air flow, and the number of active nozzles, the system is designed to deliver—on demand—continuous vapor concentrations across more than six orders of magnitude (nominally 290 fg/l to 1.05 μg/l). Vapor pulses containing femtogram to microgram quantities of analyte may also be generated. Calibrated ranges of three explosive vapors at ng/l levels were generated by the device and directly measured by ion mobility spectrometry (IMS). These data demonstrate expected linear trends within the limited working range of the IMS detector and also exhibit subtle nonlinear behavior from the IMS measurement process. © *2006 American Institute of Physics.* [DOI: 10.1063/1.2236109]

I. INTRODUCTION

The National Academies have assessed current technologies used to detect trace explosives for aviation security and the military and have called for improvements in sensitivity, selectivity, and comprehensiveness.[1,2] Next-generation detection technologies are now being developed to detect the vapors of concealed contraband (e.g., explosives, narcotics, or chemical warfare agents) that may exist only at parts-per-trillion levels (pL/L) in nearby air or in downwind air plumes. A technical barrier to this development has been the lack of a reliable and certifiable means to generate calibrated reference samples containing part-per-trillion quantities of contraband. Reference materials and methods are needed to establish tangible benchmarks for detector development, to enable intercomparison of detection technologies, and to allow quantitative verification of detector performance in the field. Verification mechanisms are also required to support the acceptance of emerging technologies by the agencies responsible for public safety and homeland security. The lack of standards has led to the development of other means to generate known concentrations of explosive vapors,[3,4] which have offered temporary recourse and are valuable as independent methods and low-cost field-portable devices.

Piezoelectric nozzles afford precise control over the microdeposition of substances, as observed in ink-jet printing and the microfabrication of microelectromechanical systems (MEMS) devices. Piezoelectric nozzles have even been used to produce aromas but have not been used, to our knowledge, for the generation of calibrated gas mixtures. The focus of this study was to develop and measure the performance of a trace vapor generator that used piezoelectric nozzles to provide air mixtures containing known ultratrace concentrations of explosive compounds.

II. EXPERIMENT AND METHODS

A. Design of the device

Design and performance specifications of the device were developed by the National Institute of Standards and Technology (NIST), and the device was built by MicroFab Technologies, Inc.[5] Principles of microdispensing technology and a brief description of the system-as-delivered have been published elsewhere.[6] At NIST, the system was customized to help characterize and enhance performance and placed in a chemical fume hood to vent the generated vapors.

The current system is shown in Figs. 1 and 2. Key features include a linear array of six piezoelectric nozzles [Fig. 1(a)] that, when sheathed in a cylindrical aluminum jacket [Fig. 1(b)], is directed at a nonporous ceramic-coated platinum resistance temperature detector (RTD) tubular element (Omega, series Kn 2 Pt 100, 25 mm heated length by 2.8 mm diameter), heated up to 250 °C under closed-loop temperature control, on the surface of which the injected droplets are vaporized. The jacket also contains six air distribution channels with filter screens. Figure 2(a) shows six reservoirs holding solutions of explosive compounds at

 © 2006 American Institute of Physics

Downloaded 06 Nov 2006 to 129.119.99.81. Redistribution subject to AIP license or copyright, see http://rsi.aip.org/rsi/copyright.jsp

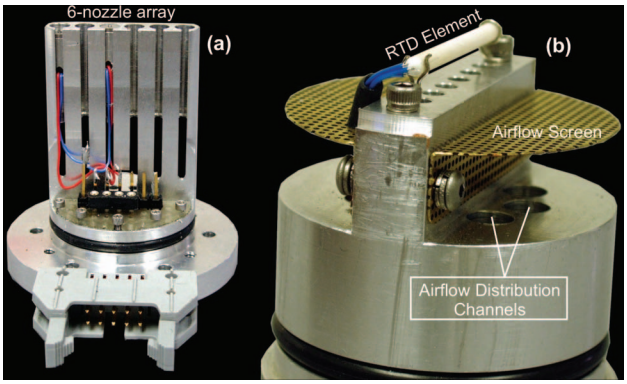

FIG. 1. (Color) The piezoelectric six-nozzle linear array (a) and array jacket (b). Here, two nozzles have been loaded in the array, which is then inserted in the jacket. When inserted, all nozzles are aimed at the ceramic tubular RTD element mounted on the jacket. The jacket also directs the calibrated airflow through six holes [three are visible in (b)] and through screens to distribute the airflow around the RTD element and promote mixing with the generated vapors.

known concentrations, which feed into the six-nozzle array through polytetrafluoroethylene (PTFE) tubing; a camera, microscope, and strobed light-emitting diode (LED) array for monitoring the microdroplet vaporization process; and a tubular glass (4.8 cm inner diameter) transition sheath that can be water cooled around the nozzle bank and heated (up to 250 °C) downstream of the vaporization area. Figure 2(b) shows a heated conduit that blends and delivers the vapor-containing air stream. Here, a commercial trace vapor detector is being tested.

By varying solution concentrations, droplet injection rates, air flow, and the number of active nozzles, the system is designed to deliver—on demand—continuous vapor concentrations across more than six orders of magnitude, while the microscope with strobed illumination verifies the delivery and vaporization of the injected droplets. Table I shows the trace vapor concentrations calculated from various combinations of the four operational parameters at maximum and minimum levels.

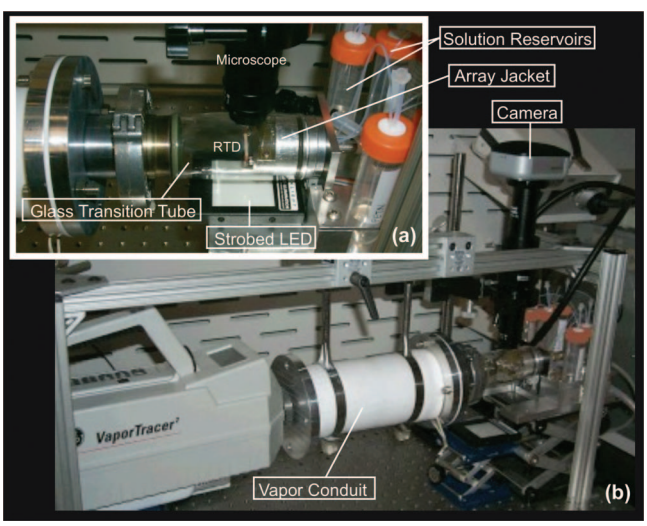

FIG. 2. (Color) Image (a) shows a microscope positioned over the 3 mm gap between the array jacket and the heated RTD within the glass transition sheath. Standard solutions are siphoned to the nozzles through PTFE tubing from 50 ml reservoirs (orange tops). The injected droplets are imaged by strobed illumination (a LED array is under the glass transition sheath) as they impinge and vaporize on the RTD. Image (b) shows the heated vapor conduit (wrapped in white insulation) from which the calibrated air stream emerges. Here, a commercial trace explosive vapor detector is positioned to sample the air stream.

B. Arrangement, monitoring, and control of the components

1. Air control

The flow of air (1–10 l/min) supplied to the device is regulated by a mass flow controller. The relative humidity (RH) of the air (10% RH to 80% RH at 25 °C) is set by passing a fixed fraction of the flow through a high-capacity bubbler and monitoring the humidity with a dew point hygrometer. The air, essentially in laminar flow conditions (Reynolds number <2000) throughout the device, enters from the rear of the aluminum array jacket and is split into six channels (each 5.0 mm long and 6.5 mm in diameter) that emerge behind a brass screen (12.0 cm^2 area, 1 mm diameter holes, and 49 holes/cm^2) designed to promote vapor/air blending in the region of the RTD element.

2. Droplet dispensing, vaporization, and monitoring

Droplet formation is controlled through the MicroFab AromaJet SMELLSERVER program (version 0.2), which sets the droplet injection wave form as well as the triggering and injection modes. To minimize costs in the prototype system, all nozzles are currently controlled through the same wave form drive electronics, so only one wave form, trigger, and mode can be selected at any one time. Although the nozzles are nominally matched so that they may be driven by the same wave form, each nozzle has a distinct optimum wave form which, in our case, requires that only one nozzle be operated at a time under the optimum wave form parameters determined for that nozzle.

A color charged-coupled-device (CCD) camera (5 Mpixels, 1.7 cm sensor size) is mounted on a microscope (magnification$=4\times-64\times$, working distance$=3.5$ cm) that is connected to an x-y-z stage at a position orthogonal to both the traveling droplets and the tubular RTD element. This position allows full viewing of droplet formation at any nozzle (Fig. 3) and droplet interaction on the surface of the RTD element. The droplets are illuminated with a backlight LED array (2.5×2.5 cm^2) powered by a strobe controller triggered by the transistor-transistor-logic (TTL) signal from the MicroFab JetDrive III nozzle driver. The digital images from the CCD camera are transmitted by IEEE 1394 (firewire) bus to a desktop computer and processed through IMAGEPRO PLUS (Media Cybernetics, v. 5.1), a program that allows collection of image sequences (up to 25 frames/s with our camera), image integration (brightness enhancement), and outline recognition (dimensional analysis). The imaged dimensions are calibrated with a reticle positioned at the focal length of the imaging system.

3. Glass transition sheath

The glass transition sheath physically adapts the nozzle head to the vapor transport tube and allows viewing of the droplet injection process. The seal around the nozzle head is made of Viton O-ring, while the other end is fitted with a

Downloaded 06 Nov 2006 to 129.119.99.81. Redistribution subject to AIP license or copyright, see http://rsi.aip.org/rsi/copyright.jsp

TABLE I. Calculated trace vapor output at extreme operational conditions.

Operational conditions				Droplet/vapor characteristics (calc.)			
Solution concentration (mg/l)	Number of active nozzles	Injection rate (Hz)	Air flow (l/m)	Droplet volume (pl)	Trace vapor concentration (pg/l)	Trace flow (pg/s)	Trace amount per droplet (fg)
10	6	3000	1	97	1 048 000	17 500	970
10	1	3000	1	97	174 600	2 910	970
10	6	50	1	97	174 600	290	970
10	1	50	1	97	2 910	48.5	970
10	6	3000	10	97	104 800	17 500	970
10	1	3000	10	97	17 500	2 910	970
10	6	50	10	97	1 750	290	970
10	1	50	10	97	290	48.5	970
0.010	6	3000	1	97	1 050	17.5	0.97
0.010	1	3000	1	97	175	2.90	0.97
0.010	6	50	1	97	17.5	0.29	0.97
0.010	1	50	1	97	2.90	0.05	0.97
0.010	6	3000	10	97	105	17.5	0.97
0.010	1	3000	10	97	17.5	2.90	0.97
0.010	6	50	10	97	1.75	0.29	0.97
0.010	1	50	10	97	0.290	0.05	0.97

63 mm i.d. International Standards Organization (ISO) flange. The ISO ends of the sheath can be heated to 250 °C with heating tape. To protect the nozzle head from heat, the front end of the sheath may be cooled with an external copper coil connected to a water-based cooling unit.

4. Vapor conduit

The vapor conduit is designed to test the transport kinetics of explosive vapors through tubing of known composition, dimensions, and temperature and to assist with blending of the vapors and calibrated airflow. The tube (304 stainless steel) is 300 cm long with an inner diameter of 2.5 cm. It is wrapped in successive layers of heating tape, fiberglass insulation, and PTFE sheeting. The tube surface temperature can exceed 250 °C, which is monitored by thermocouples mounted at several locations.

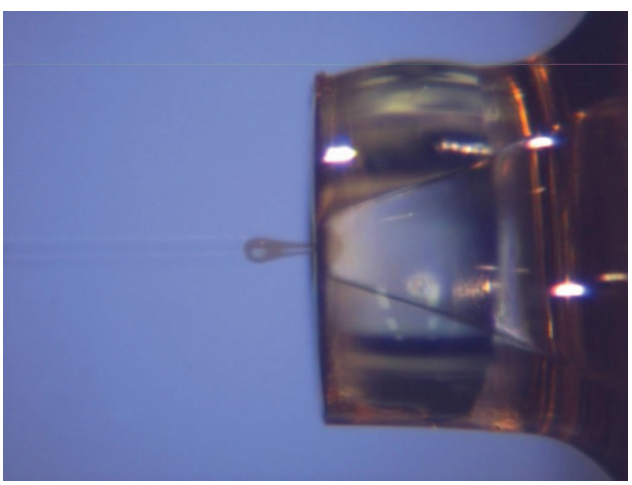

FIG. 3. (Color) An 80 μs old droplet of isobutanol (with tail), containing about 10 fg of TNT, emerges from a nozzle. Here, the head of the droplet is about 50 μm wide in the vertical direction. Droplets were injected and illuminated at 1000 Hz, and this image was collected by a CCD camera (5 Mpixels, 1.7 cm sensor) mounted on a 64× microscope.

C. Analytical methods

1. Characterization of droplet size

With the transition sheath removed, dispensed droplets of the fluid were monitored with the microscope using strobed illumination. Droplets typically emerged from the nozzles with tails or satellites that coalesced into the primary droplet. This coalescence caused small oscillations in the droplet that dissipated after about 100 μs, so we imaged the droplets after dissipation. The outline of an imaged droplet was determined by the software program, along with the average diameter of the outline and estimates of diameter uncertainty.

2. Determination of optimum wave form

The presence of maxima or minima in the droplet volume is system and fluid dependent and is a consequence of acoustic resonances in the nozzle chamber, as well as the viscosity and surface tension of the fluid. Optimum wave forms for each nozzle were determined where droplet volume was most stable and reproducible. Wave forms used to generate droplets are defined by nine time and voltage variables in the JETDRIVE program. Additional variables in the software include the trigger mode (single or continuous) and source (external or internal), number of drops per trigger, strobe delay, and the selection of active nozzles. Isobutanol (T_b=108 °C) was used as the fluid solvent because of its ability to dissolve explosive compounds, good droplet generating performance (viscosity=3.3 cP, surface tension =23 mN/m), and noninterference with our methods for explosive detection. We found that pulse amplitude, pulse width, and injection rate were most significant to the injection process, so we explored their effect on the droplet diameters from the nozzles. A fractional factorial experimental design was used having eight levels within each of the three operational variables.

Downloaded 06 Nov 2006 to 129.119.99.81. Redistribution subject to AIP license or copyright, see http://rsi.aip.org/rsi/copyright.jsp

3. Optimization of droplet vaporization

The effectiveness of the system depends on complete evaporation of the two-component fluid (analyte and solvent) after droplet injection and complete blending of the vapors with the calibrated air stream. We chose to monitor and control droplet evaporation on a RTD element rather than simply spraying droplets into the air stream. The latter would require longer residence time in the air stream to assure complete evaporation and would be susceptible to losses of droplets on surfaces as well as result in formation of aerosols rather than vapors.

The interactions of droplets with hot surfaces have been intensively studied due to significance with spray coating, fuel injection, spray cooling, and fire suppression. These studies provided guidance to system design and expectations regarding droplet impact models, boiling regimes, and Leidenfrost phenomena,[7–9] although our unique application lent some uncertainty to the expected performance. Interactions of the droplets with the surface of the RTD element were therefore observed and documented with the camera and microscope across RTD temperatures ranging from room temperature to 220 °C.

4. Testing with a trace explosive detector

The vapor transfer tube was attached to the glass-to-stainless steel transition sheath and both were heated to 200 °C. In turn, three different explosives [RDX, PETN, and TNT (Ref. 10)] as isobutanol solutions (10.0 mg/l) were dispensed at rates from 200 to 3000 Hz into 10 l/m of air, generating trace explosive concentrations of about 1.2–18.9 ng/l. The generated vapors were sampled by a Vapor Tracer 2 (VT2, GE Security) trace explosive detector operating in single gas sampling mode. In this mode, the instrument can sample and preconcentrate the vapors for various time intervals before ion mobility spectrometry (IMS) analysis, which involves an atmospheric pressure ion source, an ion-molecule reactor, an ion-drift spectrometer, and a detector.[11] The front end of the VT2 may also be fitted with a thermal desorber that allows sampling of particles and residues, and before use this instrument was calibrated for IMS drift time in this configuration using reference materials on swipes. Important to note, however, is that the associated calibration of peak response amplitude would not be equivalent between vapor sampling and particle sampling since the inlet mechanisms are different.

III. RESULTS AND DISCUSSION

A. Droplet size and optimum wave forms

Droplet diameter was measured versus pulse amplitude, pulse width, and injection frequency. For one typical nozzle, selected data (as volumes) are displayed in Fig. 4, where the vertical bars represent standard uncertainties estimated through replicated determinations of droplet diameter facilitated by the IMAGE-PRO visualization software. Figure 4(a) shows a relatively stable minimum in droplet volume (97±4 pl) at a pulse width between 38 and 42 μs. In Fig. 4(b), injection rate was varied while maintaining pulse width and amplitude at 40 μs and 40 V, respectively. Here, measurements of droplet volume were not significantly different when injected between 50 and 3000 Hz. Below 50 Hz, illumination was too low to effectively image the droplets, while at rates greater than 3000 Hz, the droplet stream became less stable with increasing production of satellite droplets. Further tuning could likely increase the operational limits, but our intention was to define a single set of wave form parameters for each nozzle that would result in reliable and reproducible operation.

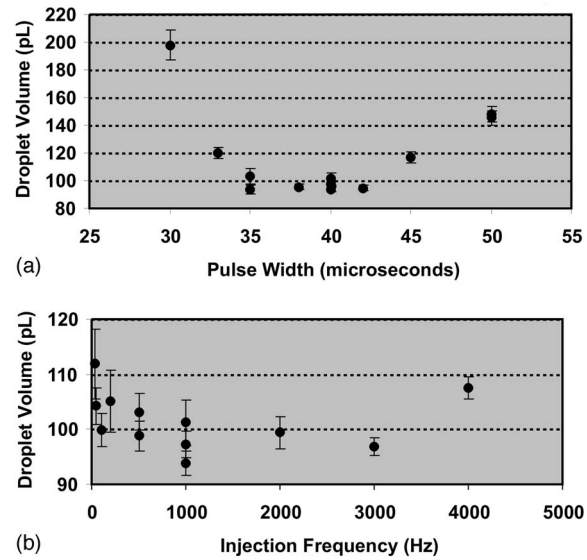

FIG. 4. Effect of piezoelectric wave form parameters on droplet volume. For a typical nozzle, plot (a) shows a relatively stable minimum in droplet volume (here, 97±4 pL) at a pulse width between 38 and 42 μs while maintaining pulse amplitude at 40 V. In plot (b), injection rate was varied while maintaining pulse width and amplitude at 40 μs and 40 V, respectively. Measurements of droplet volume were not significantly different from the value above when injecting between 50 and 3000 Hz. In both plots, the vertical bars represent standard uncertainties estimated through replicated determinations of droplet diameter performed by the IMAGE-PRO visualization software.

B. Optimization of vaporization

The microdroplets were observed to stick, rebound, or shatter off the RTD unless the RTD temperature was set to (135±5) °C, which is 27 °C above the normal boiling point of the isobutanol solvent. Only within this temperature range, where transition boiling allowed maximum heat transfer,[7] would the microdroplets vaporize completely as they impinged upon the surface. No prior studies were found for optimizing the evaporation of two-component fluid droplets where the boiling point of the trace component was substantially higher than that of the major component. Fortunately, this could be determined through thermodynamic principles, where the rate of mass flux Γ (g/m^2 s) for normal evaporation is given by Eq. (1),

$$\Gamma = \frac{m p_s}{(2\pi m k_B T)^{1/2}}. \tag{1}$$

Here, m is the mass (g) of the evaporating molecule, k_B is the Boltzmann constant (ergs/K), and p_s is the saturation vapor pressure (dyn/cm^2) at the liquid-surface temperature T (K). The saturation vapor pressure for an explosive compound

Downloaded 06 Nov 2006 to 129.119.99.81. Redistribution subject to AIP license or copyright, see http://rsi.aip.org/rsi/copyright.jsp

TABLE II. Coefficients for the reduced Clausius-Clapeyron equation [Eq. (2)] and calculated evaporation and injection rates.

Compound[a]	α (K^{-1})	β	$\Gamma_{130\,°C} \times \text{Area}$[b] (ng/s)	Λ_{max} (ng/s)
RDX	−6473	16.50	2.5	1.0[c]
PETN	−7243	19.56	42	4.2[d]
TNT	−5481	16.37	550	4.2[d]

[a]Reference 10.
[b]Droplet impingement area=2700 μm^2.
[c]Maximum allowable RDX injection rate taken as 40% of RDX evaporation rate. This rate is attained by injecting 60 μm diameter droplets of 10 mg/l RDX solution at 1000 Hz.
[d]Maximum PETN and TNT injection rates defined by upper limitation of the piezoelectric/fluid system using 10 mg/l solutions and are reached by injecting 60 μm diameter droplets at 4000 Hz.

represents the limiting droplet injection condition, and this quantity may be calculated through a reduced form of the Clausius-Clapeyron equation [Eq. (2)], with coefficients α and β (Table II) adapted from Dionne *et al.* (1986),[12]

$$\log p_s = \frac{\alpha}{T} + \beta. \tag{2}$$

The value of Γ (maximum analyte evaporation rate) over a droplet impingement area defines the upper limit of the allowed analyte injection rate Λ (g/s) per nozzle, which is calculated through Eq. (3),

$$\Lambda = CvI. \tag{3}$$

Here, C is the analyte concentration in the solvent (g/l), v is the volume of a droplet (l), and I is the droplet injection rate (Hz). For each explosive compound, values of Γ at 130 °C over a droplet impingement area (2700 μm^2) and maximum values of Λ allowed per nozzle are listed in Table II. Using 10 mg/l solutions, RDX must be limited to injection rates equal to or less than 1000 Hz (corresponding to 1.0 ng/s, 40% of saturation level). PETN and TNT have $\Gamma_{130\,°C}$ values of 42 and 550 ng/s, respectively, which are comfortably above the operating limits (4.2 ng/s) of any nozzle in our system.

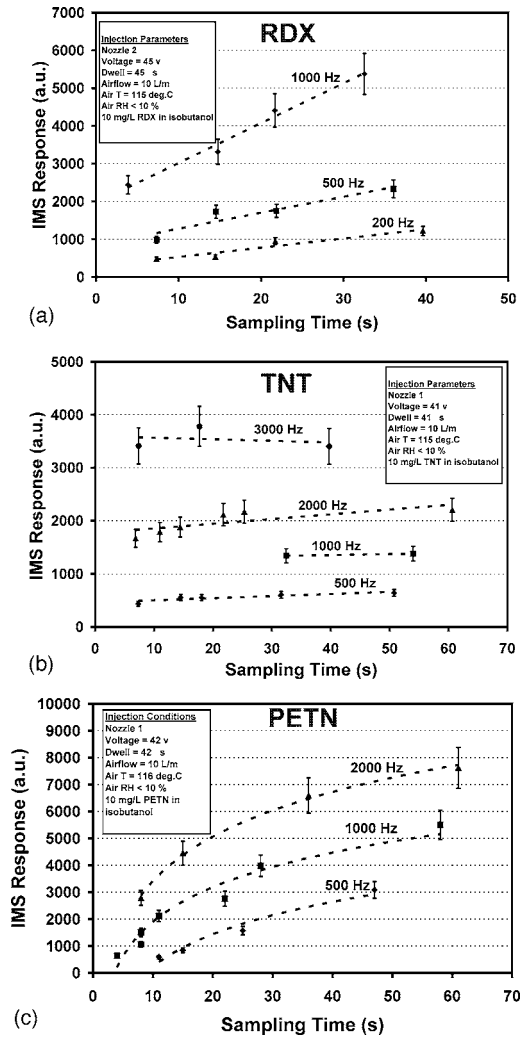

FIG. 5. Ion mobility spectrometry (IMS) measurements of RDX, TNT, and PETN vapors generated under constant air flow (10 l/m) at various injection rates. IMS measurements were performed on a GE Vapor Tracer 2 detector, where the air was sampled for durations between 3 and 65 s before IMS analysis. IMS responses to RDX (a) and PETN (c) vapors show expected dependences upon injection rate and sampling time, while IMS responses to TNT (b) vapors depended only on droplet injection rate. Data points are single analyses with analytical uncertainties estimated as 10% of the IMS signal.

C. Testing with a trace explosive detector

IMS results for explosive vapors sampled by the VT2 trace explosive detector are plotted in Fig. 5. Sampling times were measured by stopwatch and data points are single analyses with analytical uncertainties estimated as 10% of the IMS signal. IMS responses to RDX vapors [Fig. 5(a)] and PETN vapors [Fig. 5(c)] show expected dependences upon injection rate and sampling time, while IMS responses to TNT vapors [Fig. 5(b)] essentially depend only on droplet injection rate within the sampling intervals tested. The relationships between IMS response and sampling time are highly linear for RDX vapors (R^2=0.89–0.99) and fairly linear for TNT vapors (R^2=0.6–0.8) within the sampling times explored. The y intercepts are nonzero values, probably since a large fraction of the total analyte preconcentration occurs within the first second or two of sampling, after which the capacity for further preconcentration is reduced. For PETN, the relationship between IMS response and vapor sampling time is first-order logarithmic [$y=m\ln(x)+b$, where R^2 =0.95–0.99]. The PETN trend is different because this compound was measured through the nitrate ion, a thermal decomposition product of PETN. The elevated temperatures in the device, as well as the IMS inlet and drift tube, were balanced and set to allow generation and detection of many explosive compounds. At these temperatures, however, PETN nonexplosively decomposes to nitrate and other products in a multistep process.[13,14] The logarithmic relationship observed would be expected if a significant fraction of this decomposition occurred within the IMS detector. The possibility that some PETN may decompose in the vapor generator would, of course, undermine its usefulness as a calibrator for PETN. The issue might be resolved by lowering the IMS operating temperatures to allow direct measurement of PETN, but the thermal behavior of this explosive is complex and decomposition has been observed to begin at 75 °C.[15]

The data in Fig. 5 are plotted as calibration curves in

Downloaded 06 Nov 2006 to 129.119.99.81. Redistribution subject to AIP license or copyright, see http://rsi.aip.org/rsi/copyright.jsp

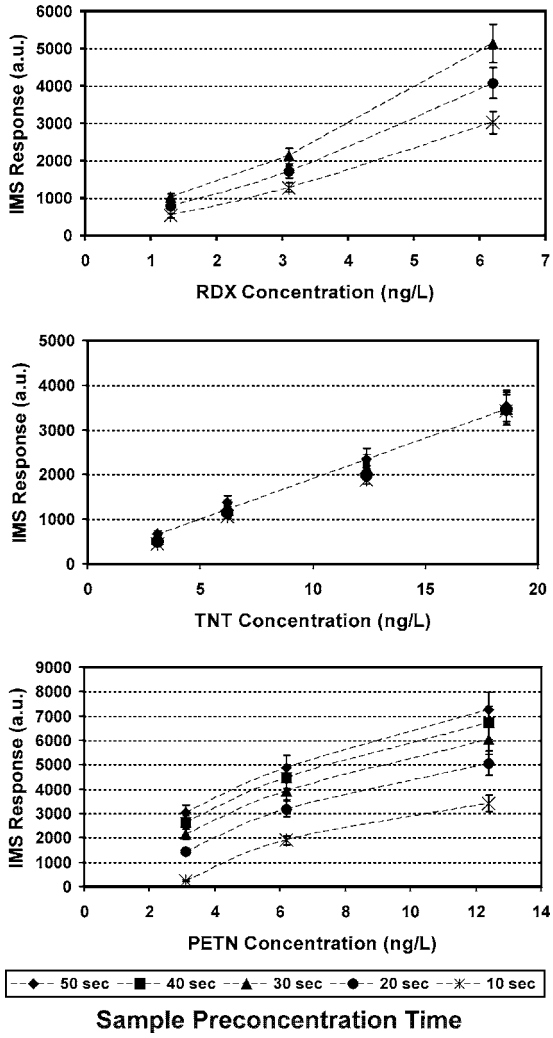

FIG. 6. Calibration curves of IMS responses to RDX (a), TNT (b), and PETN (c) vapors at discrete concentration levels and sampling times. Responses to TNT vapors were linear and independent of sampling time, while responses to RDX and PETN vapors show opposing nonlinear trends. Differences observed in these curves are probably due to the mix of nonlinear effects in sample collection efficiencies and chemical stabilities during IMS detection.

Fig. 6, where IMS response is now plotted against trace vapor concentrations at discrete sample preconcentration times. Responses to TNT vapors [Fig. 6(b)] were linear and independent of sampling time, while responses to RDX vapors [Fig. 6(a)] and PETN vapors [Fig. 6(c)] show opposing nonlinear trends. The anomalous thermal behavior of PETN leading to nonlinear effects was described above. In Fig. 6(a), the slightly convex calibration curve for RDX was not expected or easily explainable, since this trend opposes possible preconcentrator or detector saturation effects. Either this observation indicates a nonlinearity in IMS amplitude response at the RDX drift time, which may be hardware or software driven, or a nonlinearity in the output of RDX vapors at the time of the experiment. Future work will resolve the cause of this effect.

SUMMARY

We have discussed the design and demonstrated the performance of a piezoelectric trace vapor calibrator. Droplet generation and interaction with the evaporating surface may be monitored by microscope using strobed illumination, and the diameter of droplets generated and evaporated in the device is reproducible to within 4%. Using thermodynamic principles, the viability of complete evaporation of a trace analyte during observable evaporation of the droplet may be determined. We used the device to calibrate responses of a trace explosive detector to RDX, PETN, and TNT vapors at discrete levels between 1 and 20 ng/l and discussed the results.

We are currently modifying the system to study and minimize possible wall effects that may effect the concentrations delivered, especially in noncontinuous injection modes. Minor nonlinear effects associated with RDX and PETN will be investigated, and performance of the device at lower concentration levels will be further tested using independent methods available at NIST. Upon verification, the device would allow a reliable assessment of the sensitivity, selectivity, and linearity of trace chemical detectors at fg/l to ng/l concentration ranges and enable the sensor industry to pursue tangible sensitivity benchmarks and test next-generation detectors with threat-level concentrations of explosives, narcotics, and chemical weapons under controlled conditions.

ACKNOWLEDGMENTS

The Department of Homeland Security and the Transportation Security Agency are gratefully acknowledged for their support.

[1] National Materials Advisory Board, *Assessment of Technologies Deployed to Improve Aviation Security* (NRC/NAS, Washington, DC, 1999).
[2] Board on Chemical Sciences and Technology, *Existing and Potential Standoff Explosives Detection Technologies* (NRC/NAS, Washington, DC, 2004).
[3] D. S. Moore, Rev. Sci. Instrum. **75**, 2499 (2004).
[4] L. C. Buettner, U.S. Patent No. 6,722,182 (20 April 2004).
[5] Specific companies, commercial equipment, instruments, or materials are identified in this document. Such identification does not imply recommendation or endorsement by the National Institute of Standards and Technology, nor does it imply that the companies or their products identified are necessarily the best available for the purpose.
[6] D. J. Hayes and D. W. Taylor, Proc. SPIE **5778**, 368 (2005).
[7] J. D. Bernardin, C. J. Stebbins, and I. Mudawar, Int. J. Heat Mass Transfer **40**, 247 (1997).
[8] A. L. Yarin, Annu. Rev. Fluid Mech. **38**, 159 (2006).
[9] S. S. Yoon, P. E. DesJardin, C. Presser, J. C. Hewson, and C. T. Avedisian, Int. J. Multiphase Flow **32**, 132 (2006).
[10] RDX is cyclotrimethylene trinitramine ($C_3H_6N_6O_6$), also known as cyclonite and hexogen, a high explosive used in plastic explosives such as Semtex and C-4. PETN is pentaerythritol tetranitrate ($C_5H_8N_4O_{12}$), a high explosive used in Semtex and Detasheet. TNT is trinitrotoluene ($C_7H_6N_3O_6$), an explosive used in many formulations, such as Amatol and Composition B.
[11] G. A. Eiceman and Z. Karpas, *Ion Mobility Spectrometry*, 2nd ed. (CRC, Boca Raton, FL, 2004).
[12] B. C. Dionne, D. P. Rounbehler, E. K. Achter, J. R. Hobbs, and D. H. Fine, J. Energ. Mater. **4**, 447 (1986).
[13] M. A. Hiskey, K. R. Brower, and J. C. Oxley, J. Phys. Chem. **95**, 3955 (1991).
[14] C.-C. Huang and T.-S. Wu, Thermochim. Acta **204**, 239 (1992).
[15] W. L. Ng, J. E. Field, and H. M. Hauser, J. Chem. Soc., Perkin Trans. 2 **1976**, 637.

Downloaded 06 Nov 2006 to 129.119.99.81. Redistribution subject to AIP license or copyright, see http://rsi.aip.org/rsi/copyright.jsp